Gasdermin D mediates inflammation-induced defects in reverse cholesterol transport and promotes atherosclerosis.

Emmanuel Opoku[1,†], C. Alicia Traughber[1,2,3†], David Zhang[1], Amanda J Iacano[1], Mariam Khan[2,3], Juying Han[1], Jonathan D Smith[1,] and Kailash Gulshan*[1,2,3]

[1]Department of Cardiovascular and Metabolic Sciences, Cleveland Clinic, Cleveland OH 44195, USA.

[2]Center for Gene Regulation in Health and Disease, Department of Biological, Geological, and Environmental Sciences, College of Science and Health Professions, Cleveland State University, Cleveland, OH 44115, USA.

[3]Department of Biological, Geological and Environmental Sciences, Cleveland State University, Cleveland OH 44115, USA.

†Contributed equally.

*Correspondence to: Kailash Gulshan, Ph.D.

Email: k.gulshan@csuohio.edu, gulshak@ccf.org

Key Words: Cholesterol, Cardiovascular disease, Atherosclerosis, Inflammation, Gasdermin D, IL-1β,

Total Word count: 7,789

Word count of abstract: 250

Total characters with spaces: 50,770

Numbers of figures: 7

TOC category: Basic, TOC subcategory: Atherosclerosis

Abstract:

Nlrp3 inflammasome is activated in advanced human atherosclerotic plaques. Gasdermin D (GsdmD) serves as a final executor of Nlrp3 inflammasome activity, by generating membrane pores for the release of mature Interleukin-1beta (IL-1β). Inflammation dampens reverse cholesterol transport (RCT) and promotes atherogenesis, while anti-IL-1β antibodies were shown to reduce cardiovascular disease in humans. Though Nlrp3/IL-1β nexus is an emerging atherogenic pathway, the direct role of GsdmD in atherosclerosis is not yet clear. Here, we used in-vivo Nlrp3 inflammasome activation to show that the GsdmD$^{-/-}$ mice release ~80% less IL-1β vs WT mice. The GsdmD$^{-/-}$ macrophages were more resistant to Nlrp3 inflammasome mediated reduction in cholesterol efflux, showing ~26% decrease vs. ~60% reduction in WT macrophages. GsdmD expression in macrophages exacerbated foam cell formation in an IL-1β dependent fashion. The GsdmD$^{-/-}$ mice were resistance to Nlrp3 inflammasome mediated defect in RCT, with ~32% reduction in plasma RCT vs. ~ 57% reduction in WT mice, ~ 17% reduction in RCT to liver vs. 42% in WT mice, and ~ 37% decrease in RCT to feces vs. ~ 61% in WT mice. The LDLr anti-sense oligonucleotides (ASO) induced hyperlipidemic mouse model showed role of GsdmD in promoting atherosclerosis. The GsdmD$^{-/-}$ mice exhibit ~42% decreased atherosclerotic lesion area in females and ~33% decreased lesion area in males vs. WT mice. The atherosclerotic plaque-bearing WT mice showed the presence of cleaved N-terminal fragment of GsdmD, indicating cleavage of GsdmD during atherosclerosis. Our data show that GsdmD mediates inflammation-induced defect in RCT and promotes atherosclerosis.

Summary: GsdmD mediates inflammation induced defects in RCT and promotes atherosclerosis.

Non-standard abbreviations and acronyms:

ASO, antisense oligonucleotides
CAD, Coronary artery disease
CANTOS, Canakinumab Anti-Inflammatory Thrombosis Outcomes Study
GsdmD, Gasdermin D
IL-1β, Interleukin 1-beta
IL-18, Interleukin 18
LDLr, Low-density lipoprotein receptor
MACE, Major adverse coronary events
NLRP3, NOD-like receptor family pyrin domain-containing 3
NETs, Neutrophil extracellular traps
PIP2, phosphatidylinositol 4,5-bisphosphate
PS, phosphatidylserine
TLR, toll like receptor

Introduction:

The NLRP3 inflammasome is implicated in promoting CVD and metabolic diseases such as obesity-induced inflammation/insulin resistance [1, 2], and destabilization of atherosclerotic plaques [1, 3]. The Canakinumab Anti-Inflammatory Thrombosis Outcomes Study (CANTOS) trial showed that anti-IL-1β therapy reduced major adverse coronary events (MACE), independent of lipid levels [4]. The Nlrp3 inflammasome target protein "GsdmD" is involved in multiple pro-inflammatory pathways such as release of IL-1β, pyroptotic cell death, and NETosis [5, 6]. Nlrp3 inflammasome is activated in advanced human atherosclerotic plaques, but the role of GsdmD in sterile inflammatory diseases such as atherosclerosis is not yet described. Interestingly, GsdmD cleavage does not necessarily leads to pyroptotic cell death under all conditions, as GsdmD also plays a role in the release of IL-1β from living macrophages[7-9]. Thus living, but inflamed, macrophages in atherosclerotic plaques may contribute to elevate IL-1β levels in GsdmD dependent manner.

Deposition and oxidative modification of low-density lipoprotein-cholesterol (LDL-C) in the arterial intima promotes monocyte entry and transformation into macrophages, leading to lipid engulfment and foam cell formation. Foam cells become dysfunctional overtime due to unregulated lipid uptake, leading to fatty streaks and further amplification of inflammation and progression of atherosclerosis [1, 10-12]. Removal of excess cholesterol from artery wall macrophages via reverse cholesterol transport (RCT) may reverse the progression of atherosclerosis [13, 14]. Chronic inflammation serves as a double-edged sword by promoting the continued influx of immune cells into the plaque area via inducing expression of adhesion molecules such as vascular cell adhesion molecule-1 (VCAM-1) on endothelial cells, and by dampening protective RCT pathway [15, 16]. Accumulation of oxidized lipids and cholesterol crystals in plaques can engage Toll-Like Receptor (TLR) pathway and induce the assembly of

the NLRP3 inflammasome [1, 3, 12, 17]. The NLRP3 inflammasome plays a key role in processing procaspase 1 to active caspase 1, which in turn can mediate the cleavage of pro-interleukin-1β (pro-IL-1β), pro-interleukin-18 (pro-IL-18), and Gasdermin D (GsdmD) to generate active IL-1β, active IL-18, and active N-terminal fragment of GsdmD (GsdmD-NT). Mature IL-1β can be released from inflamed macrophages in at least two ways. In one pathway, the cleaved GsdmD-NT, binds to phosphatidylinositol lipids (PIPs) and phosphatidylserine (PS) on the inner leaflet of the plasma membrane of cells to generate pores for the fast release of mature IL-1β [18-20]. In the second pathway, the cleaved IL-1β exit via a slow release pathway by directly binding to the phosphatidylinositol 4,5-bisphosphate (PIP2) in plasma membrane lipid-rafts [21]. In contrast to Nlrp3 inflammasome and IL-1β, the direct role of GsdmD in atherosclerosis is not yet clear. Though GsdmD cleavage and ensuing membrane blebbing and pyroptosis is generally associated with robust release of cytokines and clearance of microbial infection, it's important to note that GsdmD also plays a role in IL-1β release from living macrophages [22]. Furthermore, similar to the apoptotic death of cholesterol-loaded macrophages [23, 24], the pyroptotic cell death can be induced by cholesterol crystals mediated Nlrp3 inflammasome activation in advanced human atherosclerotic plaques [1, 25]. Thus, GsdmD may play role in Nlrp3 inflammasome mediated dampening of RCT and in promoting the progression of atherosclerosis, either by virtue of increasing IL-1β release from live inflamed immune cells or by promoting pyroptotic cell death in advanced atherosclerotic plaques.

Results:

GsdmD$^{-/-}$ mice release lower levels of IL-1β upon in-vivo Nlrp3 inflammasome assembly.

To confirm that GsdmD $^{-/-}$ macrophages are defective in IL-1β release, primary bone-marrow-derived macrophages (BMDMs) isolated from wild type (WT) or GsdmD$^{-/-}$ mice were primed

with 1μg/ml LPS for 4h. To induce Nlrp3 inflammasome assembly, these cells were incubated with 5mM ATP for 20 min or 1 μM Nigericin for 1h, followed by a collection of cell-free media to measure released IL-1β. Consistent with previous studies, the GsdmD$^{-/-}$ macrophages showed a ~80% decrease in the release of IL-1β as compared to control macrophages (***Fig. 1A***). The basal as well as the LPS induced expression levels of NLRP3 and pro-IL-1β were not altered in GsdmD$^{-/-}$ BMDMs, indicating that only IL-1β release is defective (***Fig 1B***).

To determine the role of GsdmD in Nlrp3 inflammasome mediated IL-1β release in-vivo, the Nlrp3 inflammasome was induced in mice by i.p. injection of 5 μg LPS, followed 4h later with i.p injection of 0.5 ml of 30 mM ATP. Control mice received either saline or LPS + saline injections. The peritoneal lavage fluid was collected 30 min after ATP injection and analyzed for IL-1β levels by ELISA. As shown in ***Fig. 1C***, WT mice injected with LPS and ATP showed robust IL-1β levels in peritoneal lavage while the GsdmD$^{-/-}$ mice had a ~ 90 % reduction in IL-1β levels. The IL-1β levels were not detectable in peritoneal lavage of WT or GsdmD$^{-/-}$ mice injected with saline or LPS alone (***Fig. 1D***), showing that both LPS and ATP are required for *in vivo* Nlrp3 inflammasome activation and GsdmD is required for IL-1β release.

GsdmD$^{-/-}$ macrophages showed protection from Nlrp3 inflammasome induced defect in cholesterol efflux. To determine if Nlrp3 inflammasome activation leads to defective cholesterol efflux and if GsdmD deletion protects against this effect, cholesterol efflux assays were performed in BMDMs ± induction of Nlrp3 inflammasome. The BMDMs were labeled with ^{3}H cholesterol for 24 h, followed by induction of ABCA1 expression with liver X receptor (LXR) agonist T-0901317. The macrophages were treated ± LPS and Nigericin, followed by a chase with 5μg/ml lipid-free apoA1 for 4h. As shown in ***Fig. 2A***, LPS/Nigericin treatment of WT BMDMS led to ~ 60% decrease in cholesterol efflux vs. untreated BMDMs. The BMDMs

derived from GsdmD$^{-/-}$ KO mice showed much lower inhibition of cholesterol efflux (~26% decrease vs. untreated). The direct effect of IL-1β was evaluated by treatment of LPS treated WT or GsdmD$^{-/-}$ BMDMs with exogenous recombinant mouse IL-1β. Addition of exogenous recombinant mouse IL-1β inhibited cholesterol efflux in both WT and GsdmD$^{-/-}$ BMDM (***Fig. S1A***). To recapitulate the environment of atherosclerotic plaque area, where IL-1β released from inflamed foam cells may affect the cholesterol efflux capacity of neighboring cells, we used the conditioned media from BMDMs treated with LPS/ATP. The conditioned media from WT BMDMs inhibited cholesterol efflux in both WT and GsdmD$^{-/-}$ KO macrophages, while the conditioned media form GsdmD$^{-/-}$ BMDMs treated with LPS/ATP showed reduced suppression of cholesterol efflux (***Fig. 2B, S1B***). These data indicated that macrophages lacking GsdmD are more resistant to inflammasome-induced reduction in cholesterol efflux, mostly due to defective IL-1β release. The ABCA1 expression was pre-induced with T-compound, and as expected no significant differences in ABCA1 levels were observed in control or conditioned-media treated macrophages (***Fig. S2***). Next, we tested if IL-1β is interfering with apoA1 binding to cell membrane. The apoA1 binding to the cell-surface ± WT conditioned media was probed by using an Alexa647 labeled apoA1 as described before [26, 27]. The BMDMs showed basal apoA1 binding as they express ABCA1, albeit at low level, while induction of ABCA1 with T compound led to significant increase in apoA1 binding to the cell-surface (***Fig. 2C. 2D***). Treatment of BMDMs with WT-CM led to significant decrease in apoA1 binding to the cell-surface (***Fig. 2C, 2D***), while the GsdmD$^{-/-}$ CM media showed no effect on apoA1 binding to the cell-surface (***Fig. 2D)***.

PIP2 localization modulated GsdmD-NT mediated cell lysis. PIP2 serves as a ligand for GsdmD N-terminal (GsdmD-NT) fragment and transfection of GsdmD-NT in HEK293 cells promotes cell lysis[18]. ABCA1 expression reduces PIP2 on the inner leaflet of plasma

membrane[27, 28], thus we tested if ABCA1 expression can reduce GsdmD mediated cell lysis by transfecting the control HEK293 and HEK293-ABCA1 cells with GsdmD-NT. Transfection of GsdmD-NT, but not the full length GsdmD, caused cell lysis in HEK293 cells (***Fig. 2E***). The HEK293 cells expressing ABCA1 showed reduced cell lysis (***Fig. 2E***), indicating that PIP2 flop across the cell membrane can dampen GsdmD-NT mediated pore-formation and cell lysis. To test the direct role of PIP2 in GsdmD-NT cell lysis, we generated HEK293 cells stably expressing GFP tagged Pleckstrin homology domain of Phospholipase-C protein (2X-PH-PLC-eGFP). As the majority of cellular PIP2 is localized to the inner leaflet of plasma membrane, as expected the PH-PLC-eGFP signal was localized at the plasma membrane (***Fig. S3***).The HEK293-2X-PH-PLC-eGFP cells transfected with GsdmD-NT showed reduced lysis vs. control HEK293 cells (***Fig. 2E).*** The membrane recruitment of N-terminal GsdmD was confirmed by fractionation of cytosolic and membrane proteins using the sequential fractionation method as described earlier [29]. The membrane recruitment of GsdmD-NT was reduced in HEK-ABCA1 cells and HEK-PH-PLC cells vs. control HEK293 cells (***Fig. 2F***). These data indicated that blocking PIP2 access to NT-GsdmD reduced recruitment of GsdmD-NT to the plasma membrane, leading to lower cell lysis.

GsdmD promotes foam cell formation. To determine if the IL-1β released from inflamed cells can promote foam cell, lipid loading was performed along with treatment with conditioned media. The WT BMDMs were incubated with the conditioned media isolated from LPS+ATP treated WT or GsdmD$^{-/-}$ macrophages along with 25 μg/ml Acetylated-low-density lipoprotein (AcLDL) and 25 μg/ml oxidized low-density lipoprotein (oxLDL) for 48h to induce foam cell formation. The BMDMs were washed thoroughly with serum free media and stained with lipid-binding Nile-red dye, followed by either qualitative analysis via fluorescent microscopy or quantitative analysis via flow-cytometry. The WT BMDMs as well as the GsdmD$^{-/-}$ BMDMs

showed higher lipid accumulation in presence of WT conditioned media (***Fig. 3A, Fig. S5***). In contrast, the WT or GsdmD$^{-/-}$ BMDMs showed reduced foam cell formation with GsdmD$^{-/-}$ conditioned media treatment (***Fig. 3A, 3B)***. These data indicated that GsdmD mediated IL-1β release promote foam cell formation. Since the GsdmD$^{-/-}$ macrophages are resistant to pyroptotic cell death, we sought to determine if lipid-laden GsdmD$^{-/-}$ can instead undergo apoptotic cell death. Foam cell formation was induced by loading WT or GsdmD$^{-/-}$ BMDMs with 100 μg/ml AcLDL for 48h, followed by Nlrp3 inflammasome activation by LPS and ATP treatment. The cells were washed with PBS and the phosphatidylserine (PS) exposure at the cell-surface was determined by flow-cytometry based Annexin-Cy5 binding assay as described earlier[27]. As shown in ***Fig. 3C***, the GsdmD$^{-/-}$ foam cells showed much higher annexin V signal vs. WT foam cells (N=4, mean ± SD). These data indicated that lack of GsdmD in Nlrp3 inflammasome induced macrophages can promote apoptotic cell death in lieu of pyroptosis.

GsdmD$^{-/-}$ mice showed protection from Nlrp3 inflammasome induced defect in RCT. To determine if Nlrp3 inflammasome assembly in mice leads to defective RCT and if GsdmD$^{-/-}$ KO are protected against this effect, RCT assay was performed as described earlier [16]. The BMDMs from WT mice were loaded with acetylated-low-density lipoprotein (Ac-LDL) and radiolabeled ^{3}H cholesterol for 48 h to generate foam cells. The WT and GsdmD KO mice pretreated with LPS + ATP treatment were injected with foam cells, following the RCT assay design shown in ***Fig. 4A***. The radioactive cholesterol efflux to plasma was determined by collection of blood samples at 24h, 48h, and 72h. The liver and feces samples were collected post euthanasia and processed to determine the % of cholesterol efflux. As shown in ***Fig. 4B***, Nlrp3 inflammasome activation reduces RCT to plasma in WT mice by 67% at 24 h, by 33% at 48 h, by 47% at 72 h (Fig. 2B), while GsdmD$^{-/-}$ mice showed only 46% reduction at 24 h, 26% at 48 h, and 33% reduction at 72 h (***Fig. 4C***). The cumulative reduction in RCT to plasma in

WT mice was ~57% vs. 32% in GsdmD$^{-/-}$ mice, showing that the GsdmD$^{-/-}$ mice have 25% more preserved RCT to plasma vs. WT mice (***Fig. 4D***). The RCT to liver was reduced by 42% in WT mice vs. only 17% reduction in GsdmD$^{-/-}$ mice (***Fig. 4E***). The RCT to feces was reduced upon Nlrp3 inflammasome activation by 31% at 24 h, by 77% at 48 h, by 63% at 72 h in WT mice (***Fig. 4F***), while GsdmD$^{-/-}$ mice showed only 18% reduction at 24 h, 40% at 48 h, and 38% reduction at 72 h (***Fig. 4G***). The cumulative reduction in RCT to feces in WT mice was ~61% vs. 37% in GsdmD$^{-/-}$ mice, showing that GsdmD$^{-/-}$ mice have 24% more preserved RCT to feces vs. WT mice upon Nlrp3 inflammasome induction (***Fig. 4H***). These data indicated that GsdmD promotes inflammation-induced defects in reverse cholesterol transport.

LDLr ASO induces hyperlipidemia in WT and GsdmD$^{-/-}$ mice. Antisense oligonucleotides directed to LDLR mRNA causes hypercholesterolemia in western type diet (WTD) fed wild-type C57BL/6 mice [30]. The 12-week-old WT and GsdmD$^{-/-}$ KO mice were injected i.p with LDLr ASO or control ASO once a week for 9 weeks and mice were fed an atherogenic WTD throughout the study, as shown in atherosclerosis study design (***Fig. 5A***). The mice were weighed and plasma was collected before and after the 9-week ASO treatments, and total cholesterol (TC) levels were determined. As shown in ***Fig. 5B,*** no significant differences were found in body weight or cholesterol levels in WT and GsdmD$^{-/-}$ female mice before or after the ASO and diet interventions. The plasma TC levels showed a robust increase in LDLr ASO treated female mice and reached an average level of ~ 800 mg/dl (Fig. ***5C***). The male mice also showed similar trends with no difference in body weight gain, and increased plasma cholesterol upon LDLr ASO treatment (***Fig. 5D, 5E***). These data showed that the LDLr ASO have equivalent efficacy in both WT and GsdmD$^{-/-}$ mice.

GsdmD$^{-/-}$ mice showed reduced atherosclerosis. LDLr ASO treatment and WTD feeding leads to the development of atherosclerotic lesions in the aortic root, aortic arch, and brachiocephalic artery [30]. To determine if GsdmD plays a role in the progression of atherosclerosis, the 12-week-old WT and GsdmD$^{-/-}$ mice were injected i.p with LDLr ASO or control ASO once a week, and fed with atherogenic western type diet (WTD), to generate hyperlipidemia. The mice were sacrificed at the end of week 21 and hearts were perfused with PBS, followed by harvesting of heart, spleen, and liver. The knockdown of hepatic LDLr by the LDLr ASO was confirmed by the western blot of liver extracts (***Fig. 6A).***

The hearts were sectioned and the atherosclerotic plaques were quantified using the oil red O positive aortic root atherosclerotic lesion area. As shown in ***Fig. 6B***, WT mice injected with LDLr ASO showed large atherosclerotic lesions in both males and females, while the GsdmD$^{-/-}$ mice showed significantly smaller atherosclerotic lesions with ~42% decreased lesion area in females (***Fig. 6C***) and ~33% decreased lesion area in males (***Fig. 6D***), The WT and GsdmD$^{-/-}$ mice injected with control ASO and fed with WTD showed no atherosclerotic plaques (***Fig. S5***).

GsdmD is cleaved in atherosclerotic plaques and play role in inducing expression of adhesion molecule. To determine if GsdmD is actively cleaved in plaques, we prepared protein extracts from atherosclerotic aortas and performed western blot analysis using the antibody that recognizes only cleaved GsdmD and not the full length GsdmD. As shown in ***Fig. 7A***, the cleaved GsdmD fragments was detected in aortas of atherosclerotic WT mice. As expected, the protein extracts of aortas from GsdmD$^{-/-}$ mice showed no positive signal. To investigate mechanism of GsdmD in promoting atherosclerosis, we also probed the aortic protein extracts for VCAM-1 expression levels. The LDLr ASO injected mice showed higher expression of VCAM-1 in aortic extracts vs. control ASO injected mice (***Fig. 7A***). The aortic extracts from LDLr ASO injected GsdmD$^{-/-}$ mice showed lower induction in levels of VCAM-1

vs. WT mice, indicating that GsdmD expression induces VCAM-1 expression in hyperlipidemic mice. To further confirm the presence of cleaved GsdmD in atherosclerotic plaque areas, we performed immunohistochemistry on aortic sections and stained the tissue sections with cleaved GsdmD antibody and counterstained with hematoxylin. As shown in ***Fig. 7B***, the aortic sections from the LDLr ASO injected WT mice showed positive signal with cleaved GsdmD antibody while sections from LDLr ASO injected GsdmD$^{-/-}$ mice showed no staining. Previous study showed that the ATP levels were significantly higher in atherosclerotic LDLR$^{-/-}$ mice vs. nonatherosclerotic LDLR$^{-/-}$ mice and increased plasma ATP levels exacerbate atherosclerosis in LDLr$^{-/-}$ mice [31]. The increased plasma ATP levels can serve as danger signal and induce Nlrp3 inflammasome assembly and IL-1β release in plaques. Increased IL-1β levels can promote increased recruitment of immune cells to plaque area and promote increased ATP release from damaged foam cells due to release of cytoplasmic content. To determine if GsdmD pathway contribute to ATP release in atherosclerotic LDLR$^{-/-}$ mice, the plasma ATP levels were determined in WT and GsdmD$^{-/-}$ mice injected with LDLr ASO and fed with atherogenic diet for 9 weeks. As shown in ***Fig. 7C***, the plasma ATP increased significantly in atherosclerotic LDLR$^{-/-}$ mice while the GsdmD$^{-/-}$ LDLR$^{-/-}$ double knockout (KO) mice showed significant attenuation in levels of plasma ATP. These data indicate the decreased IL-1β release in GsdmD$^{-/-}$ LDLR$^{-/-}$ double KO mice can decrease foam cell membrane disintegration and reduce ATP release in plasma.

Discussion

Chronic inflammation is a key player in promoting atherosclerosis and cardiovascular disease [32]. The link between cholesterol efflux by ABC transporters, inflammatory cytokines, and heart disease is becoming clearer with studies showing that inflammation can promote atherosclerosis by dampening the RCT pathway [15, 33]. Many studies have highlighted the role

of Nlrp3 inflammasome/IL-1β pathway in promoting CVD [1, 3, 4, 25, 34] and the link between inflammation and CVD is further highlighted by link between sepsis survivor and higher risk of having a heart attack or stroke [35]. The role of GsdmD in sterile inflammatory diseases, such as atherosclerosis, is not yet clear. We found that in-vivo Nlrp3 inflammasome assembly in mice by LPS+ATP injections leads to GsdmD -dependent increase in IL-1β levels and reduced reverse cholesterol transport (***Fig. 1, 4***). The macrophages lacking GsdmD were more resistant to inflammation-induced defects in cholesterol efflux (***Fig. 2***). The induction of Nlrp3 inflammasome and ensuing membrane damage due to pore generation by GsdmD can reduce the cell's ability to efficiently transport cholesterol via the ABCA1-apoA1 pathway. To circumvent the membrane damage contribution towards reduced cholesterol efflux, we used conditioned media isolated from WT BMDMs treated with LPS+ATP to show can reduction in cholesterol efflux. These data pointed toward a more direct role of IL-1β in inhibiting cholesterol efflux. Binding of IL-1β to IL-1 receptor (IL-1r) may activate or block cellular signaling pathways involved in apoA1-ABCA1 cholesterol efflux pathway. The identity of this signaling pathway remains to be elucidated. Another possibility is the disruption of PIP2 trafficking in WT macrophages by the Nlrp3 inflammasome. PIP2 is translocated from the inner to outer leaflet of the plasma membrane by ABCA1 where it promotes apoA1 binding and cholesterol efflux [27]. The ABC transporter mediated PIP2 flop was confirmed by other studies [28, 36]. Cleaved GsdmD and cleaved IL-1β were reported to have PIP2 binding ability, and they may retain PIP2 on the inner leaflet and thus reduce PIP2 on the cell surface in the WT macrophages. The $GsdmD^{-/-}$ macrophages on the other hand may retain the ability to translocate PIP2 to the cell surface, and thus sustain more cholesterol efflux activity.

$GsdmD^{-/-}$ mice showed significantly reduced atherosclerosis in LDLr ASO generated hyperlipidemic mice, indicating that GsdmD promotes atherosclerosis (***Fig. 6***). GsdmD may

affect atherosclerotic plaque progression via several different mechanisms. One of the mechanisms could a simple blockage of IL-1β and IL-18 release from inflamed immune cells. This mechanism is supported by outcome of CANTOS trial showing that anti-IL-1β antibodies reduced MACE in CVD patients [4] and previous study showing role of IL-18 in atherosclerosis in mice [37]. Another mechanism by which GsdmD can promote atherosclerosis could be via regulating pyroptosis [18-20]. Unlike apoptosis, that has been main focus of studies aimed at understanding macrophage cell death in plaque area due to cholesterol overload, the role of pyroptotic cell death in atherosclerosis is not clear. The presence of cleaved N-terminal fragment of GsdmD in aortic tissue from atherosclerotic plaque-bearing mice may indicate the role of pyroptotic cell death in progression of atherosclerosis, but is not a conclusive evidence as GsdmD can also get cleaved in living macrophages [7]. The clearance of apoptotic cells by phagocytosis in plaque is of high importance as defective efferocytosis promotes further inflammation and plaque progression [38]. The pyroptotic cells may not be cleared by efferocytosis as effectively as apoptotic cells due to the lack of proper “eat-me signal”, which is exposure of phosphatidylserine (PS) on the cell-surface. Importantly, a recent study has shown existence of robust apoptotic caspase network that is activated in parallel to GsdmD-mediated plasma membrane permeabilization and shifts the balance between apoptotic and pyroptotic macrophage cell death [39]. We found that lipid-laden GsdmD KO foam cells exhibit higher apoptotic cell death vs. WT macrophages (***Fig. 3C***). Thus, KO of GsdmD may reduce atherogenic pyroptotic cell death, and may tilt the balance toward athero-protective apoptotic cell death.

Neutrophil extracellular traps (NETs) play important role in trapping extracellular pathogens but they can promote atherosclerosis by activating macrophages to release more pro-inflammatory cytokines. Hyperlipidemia and cholesterol crystals can promote formation of NETs that in turn

can play role in progression of atherosclerosis [40, 41]. Interestingly, GsdmD is also involved in NETosis and is proteolytically activated by Neutrophil proteases [5]. Thus, GsdmD KO may dampen progression of atherosclerosis due to reduced formation of NETs. Further studies are required to decipher if the GsdmD atherogenic activity is mediated solely by macrophages or other immune cells such as neutrophils, B-cells, or T-cells, also contribute to GsdmD atherogenic activity.

Our data show a novel role of GsdmD in the progression of atherosclerosis, independent of lipid levels. The idea of combining lipid-lowering therapeutics with anti-inflammatory drugs is now looking more attractive than ever [42] and targeting GsdmD in combination of LDL lowering therapies such as statins or PCSK9 antibody may serve as potential therapeutic to treat atherosclerosis and cardiovascular disease.

Material and Methods

Mice and diets: All animal experiments were performed in accordance with protocols approved by the Cleveland Clinic and Cleveland State University Institutional Animal Care and Use Committee. The C57BL6J mice were purchased from the Jackson Laboratory and the GsdmD$^{-/-}$ KO-C57BL/6J mice were generated earlier [43] and kindly provided by Dr. Russell Vance (UC, Berkeley). The GsdmD$^{-/-}$ KO genotype was confirmed by PCR & sequencing of Exon 2 of GsdmD using primers, GsdmD Fwd: ATAGAACCC GTGGAGTCCCA and GsdmD Rev: GGCTTCCCTCATTCAGTGCT as described earlier [43]. The 12-week-old mice, males and females, in C57BL/6J or GsdmD$^{-/-}$- C57BL/6J backgrounds were maintained in a temperature-controlled facility with a 12-h light/dark cycle. Mice were given free access to food and water. The standard chow diet (SD, 20% kcal protein, 70% kcal carbohydrate and 10% kcal fat, Harlan Teklad) was used for regular maintenance and breeding. For generating hyperlipidemia

for atherosclerosis studies, mice were fed an atherogenic Western type diet (WD) (ENVIGO, 0.2% cholesterol with 42% adjusted calories from fat, TD.88137).

ASO injections: GalNAc-conjugated Gen 2.5 ASO targeting mouse Low-density Lipoprotein receptor (LDLr) and control ASO were kindly provided by Adam Mullick from Ionis Pharmaceuticals. The. ASO treatment started at week 12 with i.p. injection of 5 mg/Kg body weight, 1 x per week until sacrifice at week 21. The oligo stock was prepared at 500mg/ml in sterile saline, such that a 25 g mouse would receive a 250 μl injection. The control group receive 1x per week control ASO. Following the ASO injection for 9 weeks, animals were sacrificed and hearts were perfused for sectioning for quantification of atherosclerotic lesions.

Isolation of Bone marrow derived macrophages: WT C57BL/6 or C57BL/6 *GsdmD* $^{-/-}$ *KO* mice were maintained on standard chow diet and water. Mice were euthanized by CO_2 inhalation and femoral bones were removed and flushed for marrow for isolating bone-marrow cells Detailed method for preparing bone-marrow derived macrophages is described in *Supplementary material and methods section.*

In-vivo Nlrp3 inflammasome assembly and IL-1β release assays: The 12-week-old WT or GsdmD$^{-/-}$ mice were IP injected with either 5 μg LPS, or sterile PBS. After 4h of LPS or PBS injection, the Nlrp3 inflammasome assembly in mice was induced by IP injection of ATP (0.5 ml of 30 mM, pH 7.0). The mice were euthanized after 30 min and peritoneal cavity was lavaged with 5 ml PBS. Approximately 3.5 ml peritoneal lavage fluid was recovered from each mouse and centrifuged at 15K for 10 min at room temperature. The supernatant was subjected to IL-1β ELISA, using mouse IL-1b Quantikine ELISA kit (MLB00C, R & D systems) and following manufacturer's instructions.

Cholesterol efflux assay: Cholesterol efflux assays were performed as described earlier [27]. The WT or GsdmD$^{-/-}$ BMDMs were radiolabeled with 0.5 μCi/ml of [3H]-cholesterol, ABCA1

expression in BMDMs was induced by treatment with T0901317, and chase was performed with serum free media containing cholesterol acceptor apoA1. The percent cholesterol efflux was calculated as 100 × (medium dpm) / (medium dpm + cell dpm). Detailed method is described in *Supplementary material and methods section.*

Mice RCT assay. WT Murine bone marrow derived macrophages were incubated with tritium labeled [3H] cholesterol and acetylated LDL to generate foam cells. The day prior to radiolabeled foam cell injection, mice received intraperitoneal injections of PBS or 5μg/ml LPS and three hours later mice treated with LPS received 30 mM of adenosine tri-phosphate, (sigma) pH=7.5-8. Mice received daily LPS/ATP injection through the course of the study. RCT to the plasma, liver, and feces was calculated as the % (dpm appearing in plasma/total dpm injected). Detailed method is described in *Supplementary material and methods section.*

Western blotting: BMDMs or RAW264.7 cells were grown and treated as indicated. The PBS-washed cell pellet was lysed in MPER or RIPA lysis buffer supplemented with protease inhibitors and PMSF. Detailed method is described in *Supplementary material and methods section.*

Cholesterol measurements: Total cholesterol was measured by using Stan Bio Total cholesterol reagent (#1010-225), following manufacturer's instructions.

Atherosclerotic lesion quantification: Mice were sacrificed by CO_2 inhalation and weighed at 21 weeks of age. Whole blood was collected from the retroorbital plexus into a heparinized glass capillary, mixed with EDTA and spun in a microfuge to obtain plasma. The circulatory system was perfused with 10 mL PBS and the heart was excised and preserved in 10% phosphate buffered formalin. The quantitative assessment of atherosclerotic plaque area in the aortic root was performed as previously described [44]. Lesion areas were quantified as the

mean value in multiple sections at 80 μm intervals using Image Pro software (Media Cybernetics).

Statistics. All statistics were performed using GraphPad Prism software. Comparison of two groups was performed by two-tailed *t*-test and comparison of more than two groups was performed by ANOVA with the specified posttest. Values shown are mean ± SD.

Supplementary Materials

Fig. S1. Effect of rIL-1β on cholesterol efflux and controls for Fig. 2B.

Fig. S2. ABCA1 expression in BMDMs± conditioned media.

Fig. S3. Localization of PIP2 binding PH-PLC domain in HEK293 cells stably transfected with 2X-PH-PLC-eGFP construct.

Fig. S4. Original micrograph of figure 3A.

Fig. S5. Control ASO did not generate hyperlipidemia or atherosclerotic lesions in WTD fed WT or GsdmD$^{-/-}$ KO mice.

References

1. Duewell P, Kono H, Rayner KJ, Sirois CM, Vladimer G, Bauernfeind FG, Abela GS, Franchi L, Nunez G, Schnurr M, Espevik T, Lien E, Fitzgerald KA, Rock KL, Moore KJ, Wright SD, Hornung V and Latz E. NLRP3 inflammasomes are required for atherogenesis and activated by cholesterol crystals. *Nature*. 2010;464:1357-61.
2. Vandanmagsar B, Youm YH, Ravussin A, Galgani JE, Stadler K, Mynatt RL, Ravussin E, Stephens JM and Dixit VD. The NLRP3 inflammasome instigates obesity-induced inflammation and insulin resistance. *Nat Med*. 2011;17:179-88.
3. Janoudi A, Shamoun FE, Kalavakunta JK and Abela GS. Cholesterol crystal induced arterial inflammation and destabilization of atherosclerotic plaque. *Eur Heart J*. 2016;37:1959-67.
4. Ridker PM, Everett BM, Thuren T, MacFadyen JG, Chang WH, Ballantyne C, Fonseca F, Nicolau J, Koenig W, Anker SD, Kastelein JJP, Cornel JH, Pais P, Pella D, Genest J, Cifkova R, Lorenzatti A, Forster T, Kobalava Z, Vida-Simiti L, Flather M, Shimokawa H, Ogawa H, Dellborg M, Rossi PRF, Troquay RPT, Libby P, Glynn RJ and Group CT. Antiinflammatory Therapy with Canakinumab for Atherosclerotic Disease. *N Engl J Med*. 2017;377:1119-1131.

5. Sollberger G, Choidas A, Burn GL, Habenberger P, Di Lucrezia R, Kordes S, Menninger S, Eickhoff J, Nussbaumer P, Klebl B, Kruger R, Herzig A and Zychlinsky A. Gasdermin D plays a vital role in the generation of neutrophil extracellular traps. *Sci Immunol*. 2018;3.
6. Lieberman J, Wu H and Kagan JC. Gasdermin D activity in inflammation and host defense. *Sci Immunol*. 2019;4.
7. Evavold CL, Ruan J, Tan Y, Xia S, Wu H and Kagan JC. The Pore-Forming Protein Gasdermin D Regulates Interleukin-1 Secretion from Living Macrophages. *Immunity*. 2018;48:35-44 e6.
8. Bergsbaken T, Fink SL and Cookson BT. Pyroptosis: host cell death and inflammation. *Nat Rev Microbiol*. 2009;7:99-109.
9. Ruhl S, Shkarina K, Demarco B, Heilig R, Santos JC and Broz P. ESCRT-dependent membrane repair negatively regulates pyroptosis downstream of GSDMD activation. *Science*. 2018;362:956-960.
10. Moore KJ and Tabas I. Macrophages in the pathogenesis of atherosclerosis. *Cell*. 2011;145:341-55.
11. Libby P, Ridker PM and Maseri A. Inflammation and atherosclerosis. *Circulation*. 2002;105:1135-43.
12. Tall AR and Yvan-Charvet L. Cholesterol, inflammation and innate immunity. *Nat Rev Immunol*. 2015;15:104-16.
13. Khera AV, Cuchel M, de la Llera-Moya M, Rodrigues A, Burke MF, Jafri K, French BC, Phillips JA, Mucksavage ML, Wilensky RL, Mohler ER, Rothblat GH and Rader DJ. Cholesterol efflux capacity, high-density lipoprotein function, and atherosclerosis. *N Engl J Med*. 2011;364:127-35.
14. Yvan-Charvet L, Wang N and Tall AR. Role of HDL, ABCA1, and ABCG1 transporters in cholesterol efflux and immune responses. *Arterioscler Thromb Vasc Biol*. 2010;30:139-43.
15. McGillicuddy FC, de la Llera Moya M, Hinkle CC, Joshi MR, Chiquoine EH, Billheimer JT, Rothblat GH and Reilly MP. Inflammation impairs reverse cholesterol transport in vivo. *Circulation*. 2009;119:1135-45.
16. Malik P, Berisha SZ, Santore J, Agatisa-Boyle C, Brubaker G and Smith JD. Zymosan-mediated inflammation impairs in vivo reverse cholesterol transport. *J Lipid Res*. 2011;52:951-7.
17. Razani B, Feng C, Coleman T, Emanuel R, Wen H, Hwang S, Ting JP, Virgin HW, Kastan MB and Semenkovich CF. Autophagy links inflammasomes to atherosclerotic progression. *Cell Metab*. 2012;15:534-44.
18. Liu X, Zhang Z, Ruan J, Pan Y, Magupalli VG, Wu H and Lieberman J. Inflammasome-activated gasdermin D causes pyroptosis by forming membrane pores. *Nature*. 2016;535:153-8.
19. Ding J, Wang K, Liu W, She Y, Sun Q, Shi J, Sun H, Wang DC and Shao F. Pore-forming activity and structural autoinhibition of the gasdermin family. *Nature*. 2016;535:111-6.
20. Kayagaki N, Stowe IB, Lee BL, O'Rourke K, Anderson K, Warming S, Cuellar T, Haley B, Roose-Girma M, Phung QT, Liu PS, Lill JR, Li H, Wu J, Kummerfeld S, Zhang J, Lee WP, Snipas SJ, Salvesen GS, Morris LX, Fitzgerald L, Zhang Y, Bertram EM, Goodnow CC and Dixit VM. Caspase-11 cleaves gasdermin D for non-canonical inflammasome signalling. *Nature*. 2015;526:666-71.
21. Monteleone M, Stanley AC, Chen KW, Brown DL, Bezbradica JS, von Pein JB, Holley CL, Boucher D, Shakespear MR, Kapetanovic R, Rolfes V, Sweet MJ, Stow JL and Schroder K. Interleukin-1beta Maturation Triggers Its Relocation to the Plasma Membrane for Gasdermin-D-Dependent and -Independent Secretion. *Cell Rep*. 2018;24:1425-1433.

22. Evavold CL, Ruan J, Tan Y, Xia S, Wu H and Kagan JC. The Pore-Forming Protein Gasdermin D Regulates Interleukin-1 Secretion from Living Macrophages. *Immunity*. 2017.
23. Feng B, Yao PM, Li Y, Devlin CM, Zhang D, Harding HP, Sweeney M, Rong JX, Kuriakose G, Fisher EA, Marks AR, Ron D and Tabas I. The endoplasmic reticulum is the site of cholesterol-induced cytotoxicity in macrophages. *Nat Cell Biol*. 2003;5:781-92.
24. Liao X, Sluimer JC, Wang Y, Subramanian M, Brown K, Pattison JS, Robbins J, Martinez J and Tabas I. Macrophage autophagy plays a protective role in advanced atherosclerosis. *Cell Metab*. 2012;15:545-53.
25. Rajamaki K, Lappalainen J, Oorni K, Valimaki E, Matikainen S, Kovanen PT and Eklund KK. Cholesterol crystals activate the NLRP3 inflammasome in human macrophages: a novel link between cholesterol metabolism and inflammation. *PLoS One*. 2010;5:e11765.
26. Wang S, Gulshan K, Brubaker G, Hazen SL and Smith JD. ABCA1 mediates unfolding of apolipoprotein AI N terminus on the cell surface before lipidation and release of nascent high-density lipoprotein. *Arterioscler Thromb Vasc Biol*. 2013;33:1197-205.
27. Gulshan K, Brubaker G, Conger H, Wang S, Zhang R, Hazen SL and Smith JD. PI(4,5)P2 Is Translocated by ABCA1 to the Cell Surface Where It Mediates Apolipoprotein A1 Binding and Nascent HDL Assembly. *Circ Res*. 2016;119:827-38.
28. Vivas O, Tiscione SA, Dixon RE, Ory DS and Dickson EJ. Niemann-Pick Type C Disease Reveals a Link between Lysosomal Cholesterol and PtdIns(4,5)P2 That Regulates Neuronal Excitability. *Cell Rep*. 2019;27:2636-2648 e4.
29. Baghirova S, Hughes BG, Hendzel MJ and Schulz R. Sequential fractionation and isolation of subcellular proteins from tissue or cultured cells. *MethodsX*. 2015;2:440-5.
30. Basu D, Hu Y, Huggins LA, Mullick AE, Graham MJ, Wietecha T, Barnhart S, Mogul A, Pfeiffer K, Zirlik A, Fisher EA, Bornfeldt KE, Willecke F and Goldberg IJ. Novel Reversible Model of Atherosclerosis and Regression Using Oligonucleotide Regulation of the LDL Receptor. *Circ Res*. 2018;122:560-567.
31. Stachon P, Geis S, Peikert A, Heidenreich A, Michel NA, Unal F, Hoppe N, Dufner B, Schulte L, Marchini T, Cicko S, Ayata K, Zech A, Wolf D, Hilgendorf I, Willecke F, Reinohl J, von Zur Muhlen C, Bode C, Idzko M and Zirlik A. Extracellular ATP Induces Vascular Inflammation and Atherosclerosis via Purinergic Receptor Y2 in Mice. *Arterioscler Thromb Vasc Biol*. 2016;36:1577-86.
32. Nissen SE, Nicholls SJ, Sipahi I, Libby P, Raichlen JS, Ballantyne CM, Davignon J, Erbel R, Fruchart JC, Tardif JC, Schoenhagen P, Crowe T, Cain V, Wolski K, Goormastic M, Tuzcu EM and Investigators A. Effect of very high-intensity statin therapy on regression of coronary atherosclerosis: the ASTEROID trial. *JAMA*. 2006;295:1556-65.
33. Yvan-Charvet L, Ranalletta M, Wang N, Han S, Terasaka N, Li R, Welch C and Tall AR. Combined deficiency of ABCA1 and ABCG1 promotes foam cell accumulation and accelerates atherosclerosis in mice. *J Clin Invest*. 2007;117:3900-8.
34. van der Heijden T, Kritikou E, Venema W, van Duijn J, van Santbrink PJ, Slutter B, Foks AC, Bot I and Kuiper J. NLRP3 Inflammasome Inhibition by MCC950 Reduces Atherosclerotic Lesion Development in Apolipoprotein E-Deficient Mice-Brief Report. *Arterioscler Thromb Vasc Biol*. 2017;37:1457-1461.
35. Lai CC, Lee MG, Lee WC, Chao CC, Hsu TC, Lee SH, Lee CC and National Taiwan University Hospital Health Data Science Research G. Susceptible period for cardiovascular complications in patients recovering from sepsis. *CMAJ*. 2018;190:E1062-E1069.
36. Deppe JP, Rabbat R, Hortensteiner S, Keller B, Martinoia E and Lopez-Marques RL. The wheat ABC transporter Lr34 modifies the lipid environment at the plasma membrane. *J Biol Chem*. 2018;293:18667-18679.

37. Whitman SC, Ravisankar P and Daugherty A. Interleukin-18 enhances atherosclerosis in apolipoprotein E(-/-) mice through release of interferon-gamma. *Circ Res*. 2002;90:E34-8.
38. Kasikara C, Doran AC, Cai B and Tabas I. The role of non-resolving inflammation in atherosclerosis. *J Clin Invest*. 2018;128:2713-2723.
39. de Vasconcelos NM, Van Opdenbosch N, Van Gorp H, Martin-Perez R, Zecchin A, Vandenabeele P and Lamkanfi M. An Apoptotic Caspase Network Safeguards Cell Death Induction in Pyroptotic Macrophages. *Cell Rep*. 2020;32:107959.
40. Warnatsch A, Ioannou M, Wang Q and Papayannopoulos V. Inflammation. Neutrophil extracellular traps license macrophages for cytokine production in atherosclerosis. *Science*. 2015;349:316-20.
41. Doring Y, Libby P and Soehnlein O. Neutrophil Extracellular Traps Participate in Cardiovascular Diseases: Recent Experimental and Clinical Insights. *Circ Res*. 2020;126:1228-1241.
42. Ridker PM. From CANTOS to CIRT to COLCOT to Clinic: Will All Atherosclerosis Patients Soon Be Treated With Combination Lipid-Lowering and Inflammation-Inhibiting Agents? *Circulation*. 2020;141:787-789.
43. Rauch I, Deets KA, Ji DX, von Moltke J, Tenthorey JL, Lee AY, Philip NH, Ayres JS, Brodsky IE, Gronert K and Vance RE. NAIP-NLRC4 Inflammasomes Coordinate Intestinal Epithelial Cell Expulsion with Eicosanoid and IL-18 Release via Activation of Caspase-1 and -8. *Immunity*. 2017;46:649-659.
44. Baglione J and Smith JD. Quantitative assay for mouse atherosclerosis in the aortic root. *Methods Mol Med*. 2006;129:83-95.

Author Contributions

K.G. designed and directed research. E.O, C.A.T, D.Z, A.J.I, J.H, M.K. and K.G performed research. E.O, C.A.T, J.D.S, and K.G. analyzed data. K.G. drafted the manuscript. All authors critically reviewed the manuscript.

Acknowledgments

This work was supported by National Institutes of Health Grant RO1HL148158 (to K.G), American Heart Association Scientist Development Grant SDG25710128 (to K.G), and Cleveland State University startup funds (to K.G.). C.A.T is supported by F31HL134231 and J.D.S is supported by RO1HL128268 and R01 HL130085.

Disclosures None.

Figure legends:

Fig. 1. A) **GsdmD plays a role in release of mature IL-1β upon in-vivo Nlrp3 inflammasome activation.** ***A***) BMDMs isolated from WTC57BL/6J or C57BL6/J-GsdmD$^{-/-}$ mice were primed by incubation with ± 1μg/ml LPS for 4h. The Nlrp3 inflammasome assembly was induced either by incubation with 1 mM ATP for 20 min or 1μM Nigericin for 1h . The IL-1β levels in the cell-free media were measured by ELISA (mean ± SD, N = 6, *** represent p<0.001 by ANOVA with Bonferroni posttest). ***B***) WT or GsdmD$^{-/-}$ BMDMs were treated ± 1μg/ml LPS, followed by western blot analysis using Nlrp3 and-IL-1β antibodies. The β-actin was used as a loading control. ***C***) The age-matched male WTC57BL/6J or GsdmD$^{-/-}$ mice were primed with IP injection of LPS (5μg/mouse). After 4h of LPS injection, the Nlrp3 inflammasome assembly in mice was induced by IP injection of ATP (0.5 ml of 30 mM, pH 7.0). The peritoneal cavity was lavaged with 3 ml PBS, and IL-1β levels in peritoneal lavage were determined by ELISA (N=6, **** p <0.0001 by two-tailed t-test). **D**) The age-matched male WTC57BL/6J or GsdmD$^{-/-}$ mice were treated with ± IP injection of LPS (5μg/mouse) and injected with 0.5 ml of saline. The peritoneal cavity was lavaged with 5 ml PBS, and IL-1β levels in peritoneal lavage were determined by ELISA (N=4, n.s.=non-significant by two-tailed t-test).

Fig. 2 GsdmD promotes Nlrp3 inflammasome-mediated defects in reverse cholesterol transport. ***A***) BMDMs isolated from WT or GsdmD$^{-/-}$ mice were loaded with ^{3}H-cholesterol + 50μg/ml AcLDL for 24h and treated with LXR-agonist T0901317 (Sigma-Aldrich) to induce ABCA1 expression. The Nlrp3 inflammasome was induced by LPS+ Nigericin treatment, followed by cholesterol efflux assay using lipid-free apoA1 (5μg/ml) in serum-free DMEM as chase media for 4h at 37^{o}C. Values are % cholesterol efflux (mean ± SD, N = 4, **** represent p<0.00011, ** represent p<0.01 by ANOVA Bonferroni posttest). ***B***) The BMDMs isolated from WT or GsdmD$^{-/-}$ mice were loaded with ^{3}H-cholesterol + 50μg/ml AcLDL for 24h. The BMDMs, ± LXR-agonist T0901317, were treated with conditioned media isolated from LPS+ATP treated WT or GsdmD$^{-/-}$ BMDMs for 16h. The cholesterol efflux assay was performed using lipid-free apoA1 (5μg/ml) in serum-free DMEM as chase media for 4h at 37^{o}C. Values are % cholesterol efflux (mean ± SD, N = 4, **** represent p<0.00011, *** represent p<0.001 by ANOVA Bonferroni posttest). ***C***) The flow cytometry analysis showing histogram bar for Alexa-647 labeled apoA1 binding to cells, ± ABCA1 expression and ± WT conditioned media treatment ***D***) The flow cytometry analysis showing quantification of Alexa-647 labeled apoA1 binding to cells ± ABCA1 expression and ±. WT or GsdmD$^{-/-}$ conditioned media treatment (mean ± SD, N = 4, **** represent p<0.00011, *** represent p<0.001 by ANOVA Bonferroni posttest) ***E***) The HEK293, HEK293-ABCA1-eGFP, or HEK293-2X-PH-PLC-eGFP cells were transfected with plasmids carrying either full-length (FL) GsdmD or N-terminal fragment (NT) of GsdmD. The LDH release in media is plotted in % values of total cellular LDH (mean ± SD, N = 4; different letters show p<0.001, by ANOVA Bonferroni posttest). ***F***) The control HEK293 and HEK293 cells stably transfected with ABCA1 or PH-PLC were transfected with plasmid carrying Flag tagged GsdmD-NT. The transfected cells were fractionated into cytoplasmic or membrane bound fractions. The fractions were resolved using SDS gel, transferred to nitrocellulose membrane, and probed with antibody against Flag tag.

Fig. 3 GsdmD promotes foam cell formation. ***A***) BMDMs isolated from WT or GsdmD$^{-/-}$ mice were loaded with 50μg/ml AcLDL + 25μg/ml OxLDL for 48 h ± conditioned media isolated from LPS/ATP treated WT or GsdmD$^{-/-}$ BMDMs. The culture media was removed, cells were washed

with PBS, and stained with Nile-red dye (0.25 μg/ml) at 37°C for 15 min. The stained cells were washed thoroughly with PBS and fixed with paraformaldehyde and imaged using fluorescent microscope with TRITC filter (Excitation / emission: 550 / 640 nm). ***B***) Quantification of Nile-red staining in WT or GsdmD$^{-/-}$ BMDMs ± conditioned media by flow-cytometry, mean ± SD, N = 4, **** represent p<0.0001 by ANOVA Bonferroni posttest. ***C***) BMDMs isolated from WT or GsdmD$^{-/-}$ mice were loaded with 50μg/ml AcLDL + 25μg/ml OxLDL for 48 h. The foam cells were left untreated or treated with LPS+ATP to induce Nlrp3 inflammasome. The cells were washed with PBS, and PS exposure was determined by flow-cytometry based assay using Annexin Cy5 staining (mean ± SD, N = 4, **** represent p<0.00011, *** represent p<0.001 by ANOVA Bonferroni posttest, n.s=non-significant).

Fig. 4: GsdmD mediates Nlrp3 inflammasome-induced defects in reverse cholesterol transport. ***A***) Schematic representation of mouse RCT study design. The 12-week-old male mice were injected daily with or without 5ug LPS and 30mM ATP for 4 days. On day 2 mice were injected with radiolabeled foam cells loaded with AcLDL and ^{3}H cholesterol. The plasma and feces RCT was assessed at 24,48,72h (quantified as a % of the 24h Ctrl for each group) and cumulatively (quantified as a percent of respective Ctrl). ***B***) RCT to plasma in WT mice at 24h, 48h, and 72h. ***C***) RCT to plasma in GsdmD$^{-/-}$ mice at 24h, 48h, and 72h. ***D***) Cumulative RCT to plasma in WT and GsdmD$^{-/-}$ mice. ***E***) RCT to liver in WT and GsdmD$^{-/-}$ mice. ***F***) RCT to feces in WT mice at 24h, 48h, and 72h. ***G***) RCT to feces in GsdmD$^{-/-}$ mice at 24h, 48h, and 72h. ***H***) Cumulative RCT to feces in WT and GsdmD$^{-/-}$ mice. N=4-5, for WT and GsdmD$^{-/-}$ Ctrl mice, N=6-7 for WT and GsdmD$^{-/-}$ LPS/ATP mice. ****p<0.0001, ***p<0.001, **p<0.01 by two-tailed t-test. Groups with different letters a, b, c, d is p<0.05 by One-way ANOVA.

Fig. 5. ***LDLr ASO generates hyperlipidemia in both WT and GsdmD$^{-/-}$ KO mice. A***) Schematic representation of mouse atherosclerosis study design. The 12-week-old mice from both sexes were injected with either control or LDLr ASO for 9 weeks. The mice were fed western type diet throughout the course of study. The body weight in females (***B***) and total plasma cholesterol levels (***C***) at week 0 and at the end of experiment, indicated by week 9, (mean ± SD, N = 12, **** p <0.0001 by two-tailed t-test, n.s= non-significant), and male data for body weight (**D**) and total plasma cholesterol levels (***E***) is presented at base and final levels (N=12 **** p <0.0001 by two-tailed t-test for both WT-week 0 vs. WT-week 9 and GsdmD$^{-/-}$-week 0 vs. GsdmD$^{-/-}$-week 9 , n.s= non-significant by two-tailed t-test).

Fig. 6. GsdmD promotes atherosclerosis and is cleaved in atherosclerotic plaques. The 12-weeks old mice from both sexes were injected with either control or LDLr ASO for 9 weeks and were fed western type diet throughout the course of study. Mice were euthanized after 9-week ASO treatment and were perfused with PBS and hearts and livers were removed. ***A)*** A small portion of liver from mice was excised, weighed, and protein extracts were prepared using RIPA buffer supplemented with protease inhibitors. Western blot analysis of LDLr in liver extracts was performed using LDLr antibody and HRP conjugated secondary antibody. ***B)*** Representative images from both sexes showing aortic root lesions stained with Oil red O and hematoxylin from WT or GsdmD$^{-/-}$ KO mice injected with LDLr ASO and fed WTD,. ***C, D)*** Quantification of aortic root lesions in females and males from WT or GsdmD$^{-/-}$ KO mice treated with LDLr ASO and fed WTD (for WT male N=11, for WT females, GsdmD$^{-/-}$ males, and GsdmD$^{-/-}$females, N=12, *** p <0.0005, **** p<0.0001 by two-tailed t-test).***E)*** Protein extracts from aortas of control ASO or LDLr ASO treated mice (N=4) were subjected to western blot analysis using antibody specific for cleaved GsdmD and VCAM-1. GAPDH was probed as a

loading control. ***F)*** ATP levels in plasma of control ASO or LDLr ASO treated mice fed with atherogenic diet were determined by ATP quantification kit, following manufacturer's instructions. (mean ± SD, N = 8; different letters show $p<0.001$, by ANOVA Bonferroni posttest).

Fig. 7. GsdmD is cleaved in atherosclerotic plaques. A) The 12-weeks old mice were injected with either control or LDLr ASO for 9 weeks and were fed western type diet throughout the course of study. Mice were euthanized after 9-week ASO treatment and protein extracts from aortas of control ASO or LDLr ASO treated mice (N=4) were subjected to western blot analysis using antibody specific for cleaved GsdmD and VCAM-1. GAPDH was probed as a loading control. ***B)*** The fresh Frozen hearts were sectioned, followed by antigen retrieval and endogenous peroxidase activity blocking, and probing with antibody specific for cleaved N-terminal fragment of Gasdermin D. ***C)*** ATP levels in plasma of control ASO or LDLr ASO treated mice fed with atherogenic diet were determined by ATP quantification kit, following manufacturer's instructions. (mean ± SD, N = 8; different letters show $p<0.001$, by ANOVA Bonferroni posttest).

Figure 1

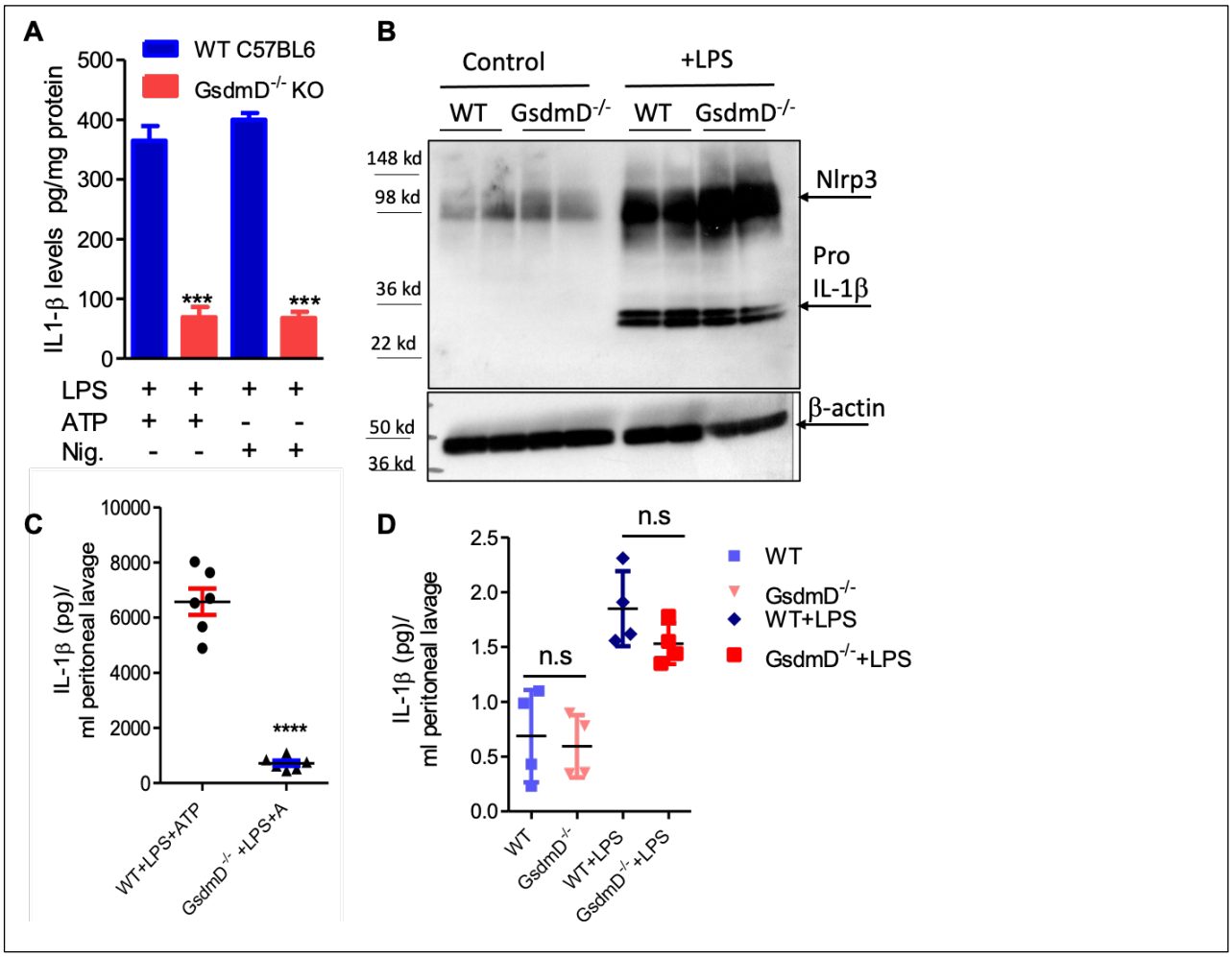

Figure 2

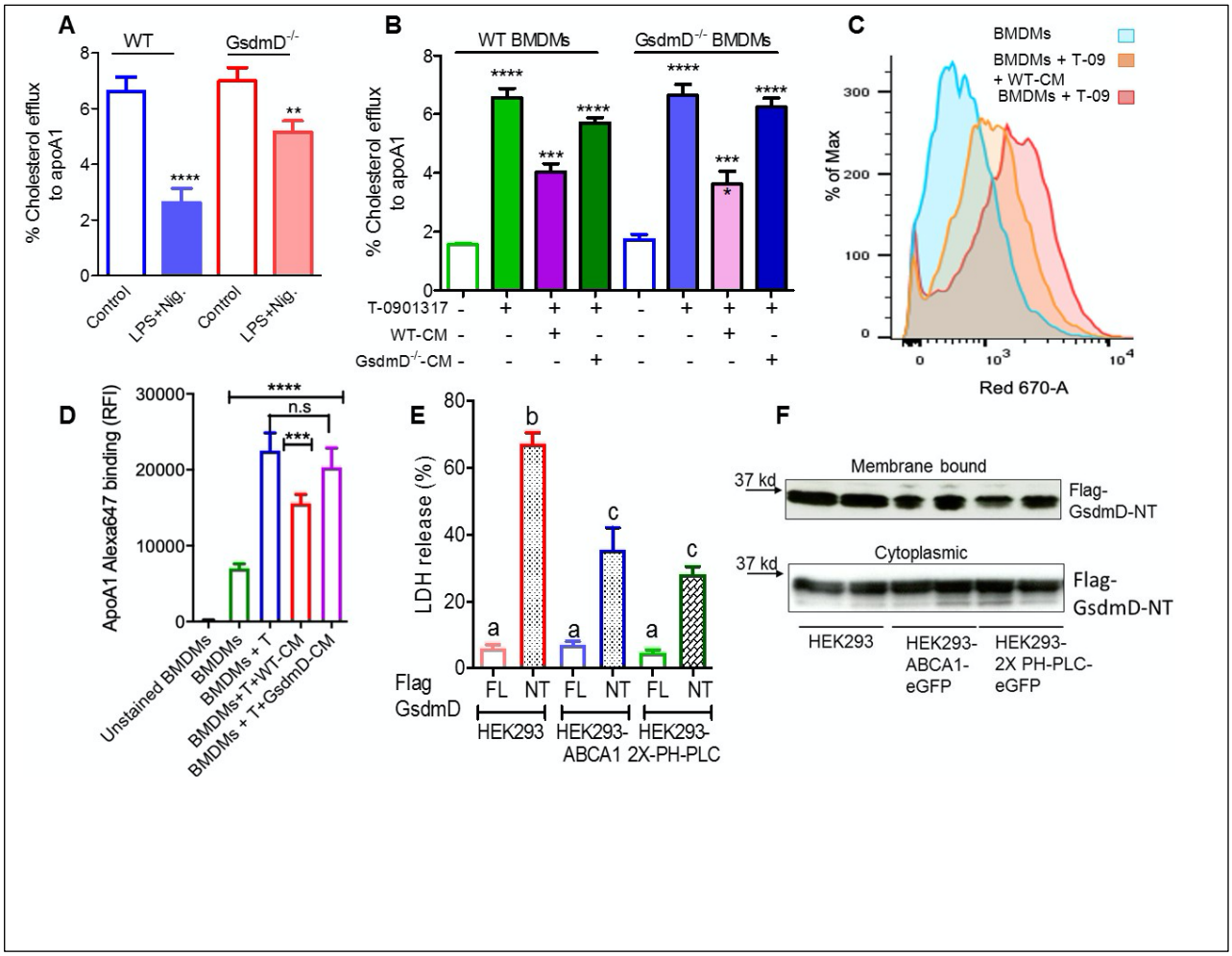

Figure 3

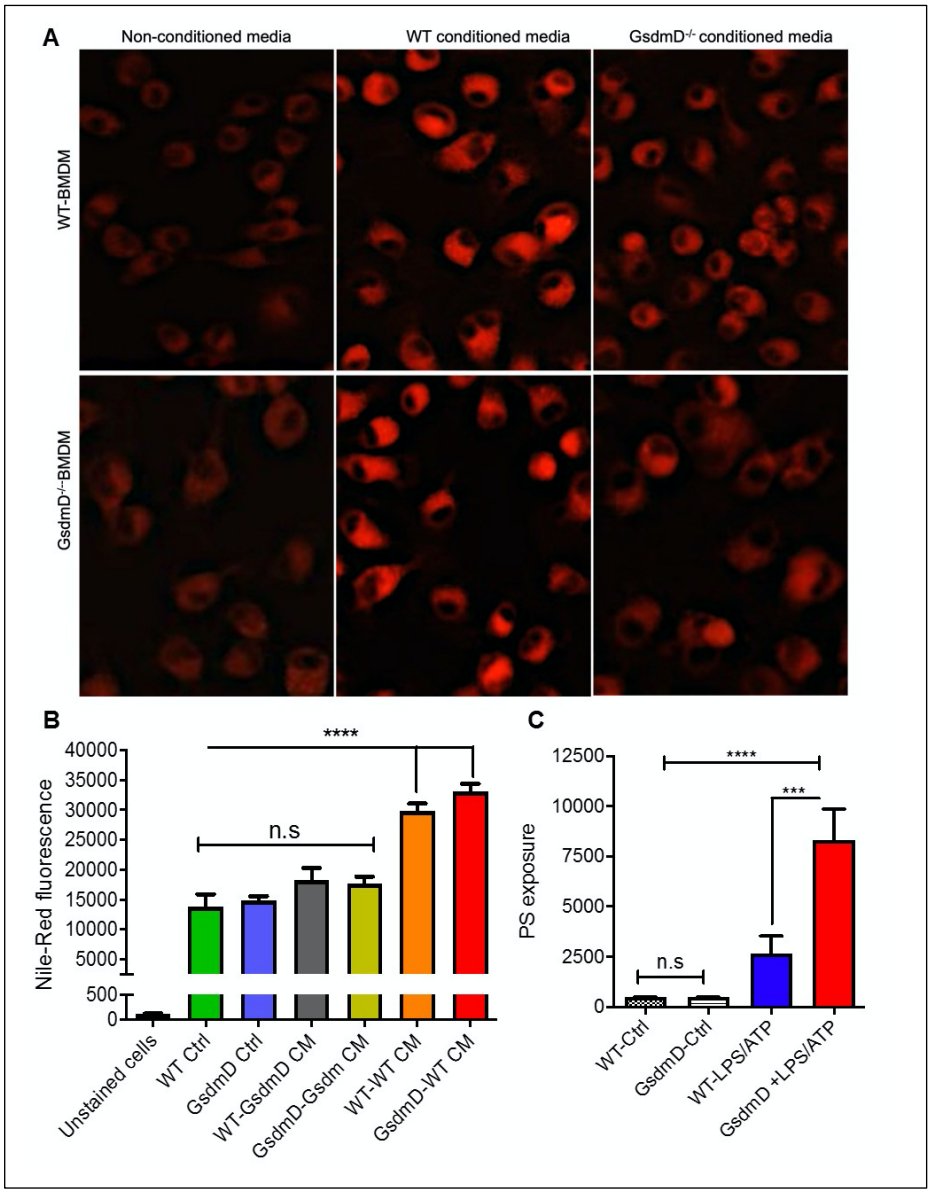

Figure 4

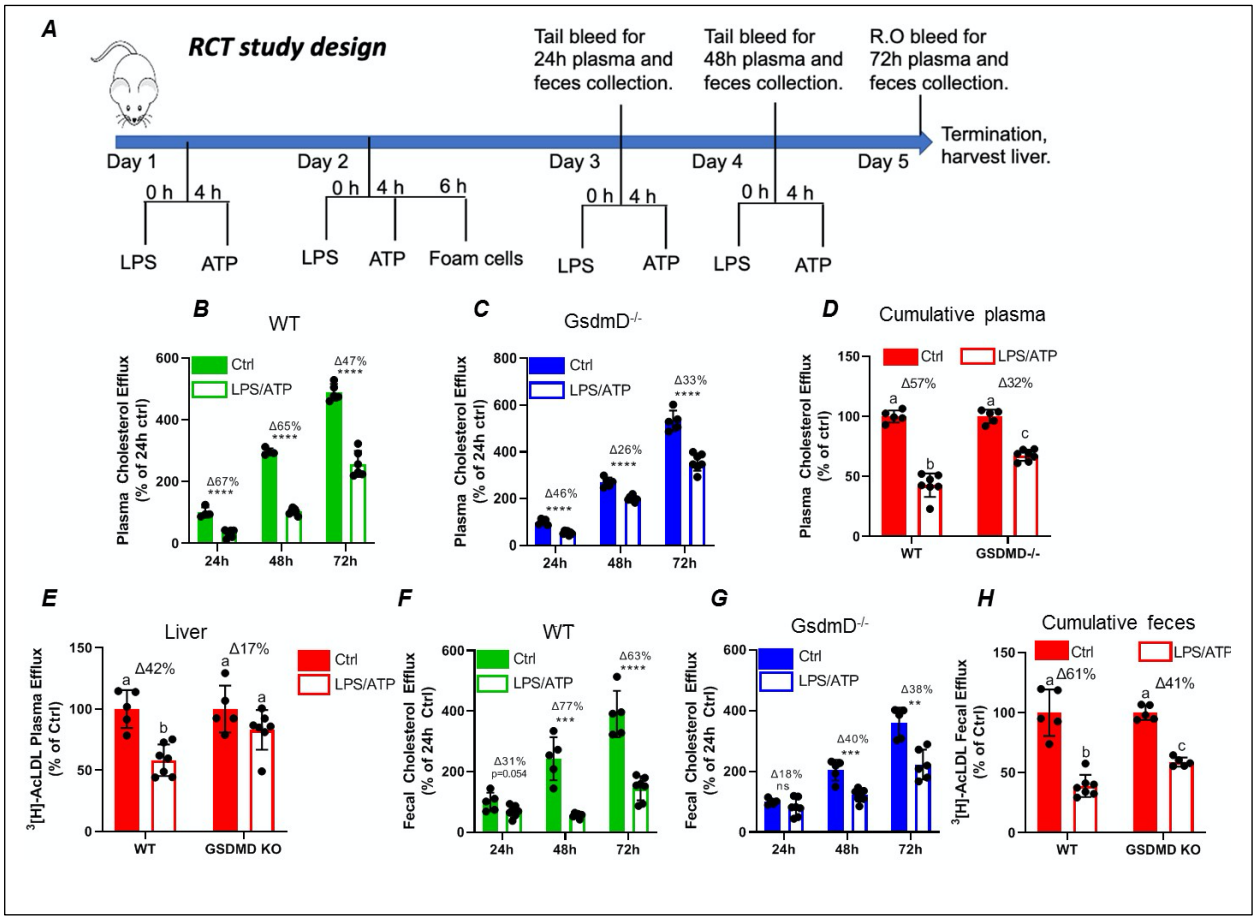

Figure 5

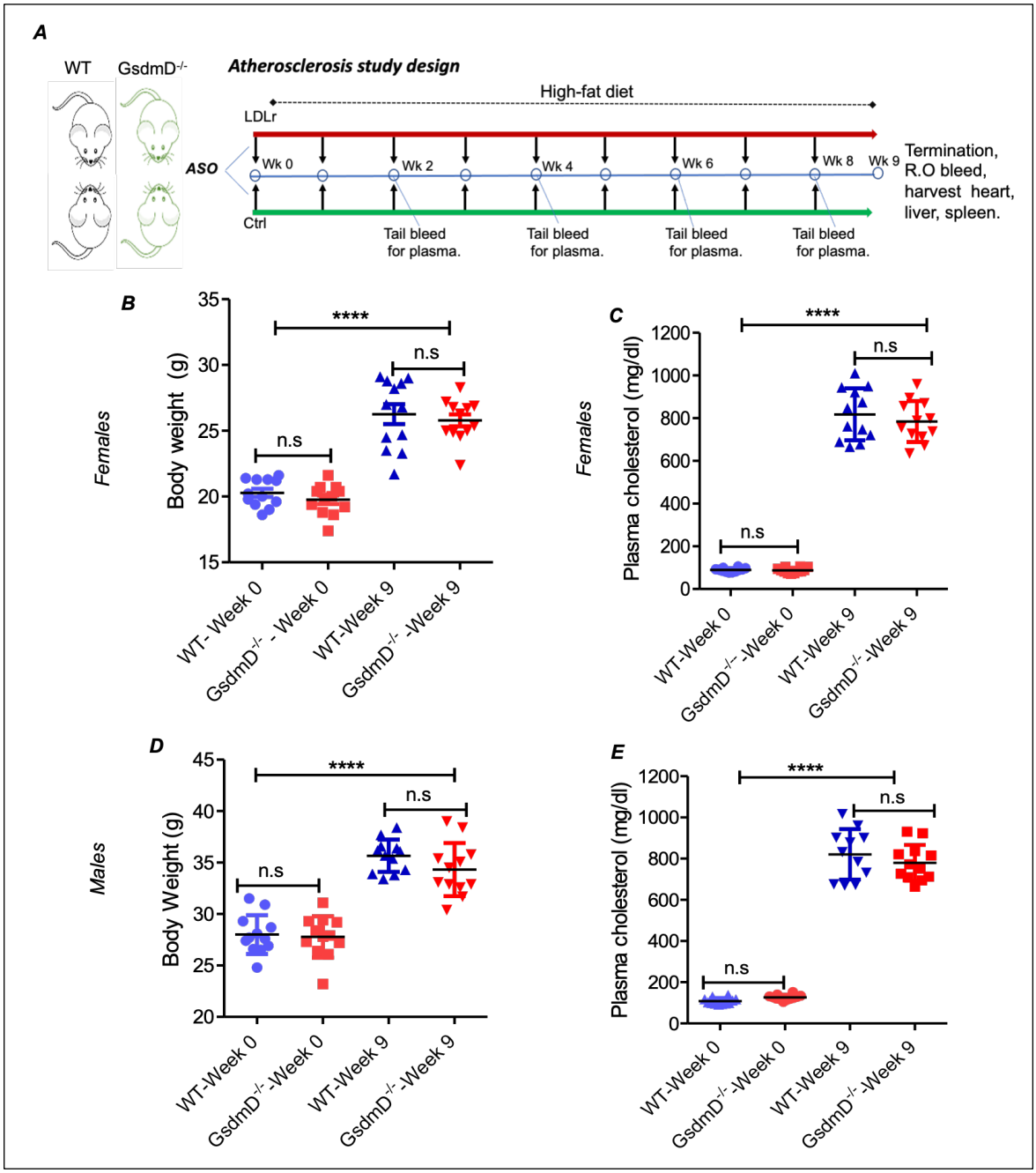

Figure 6

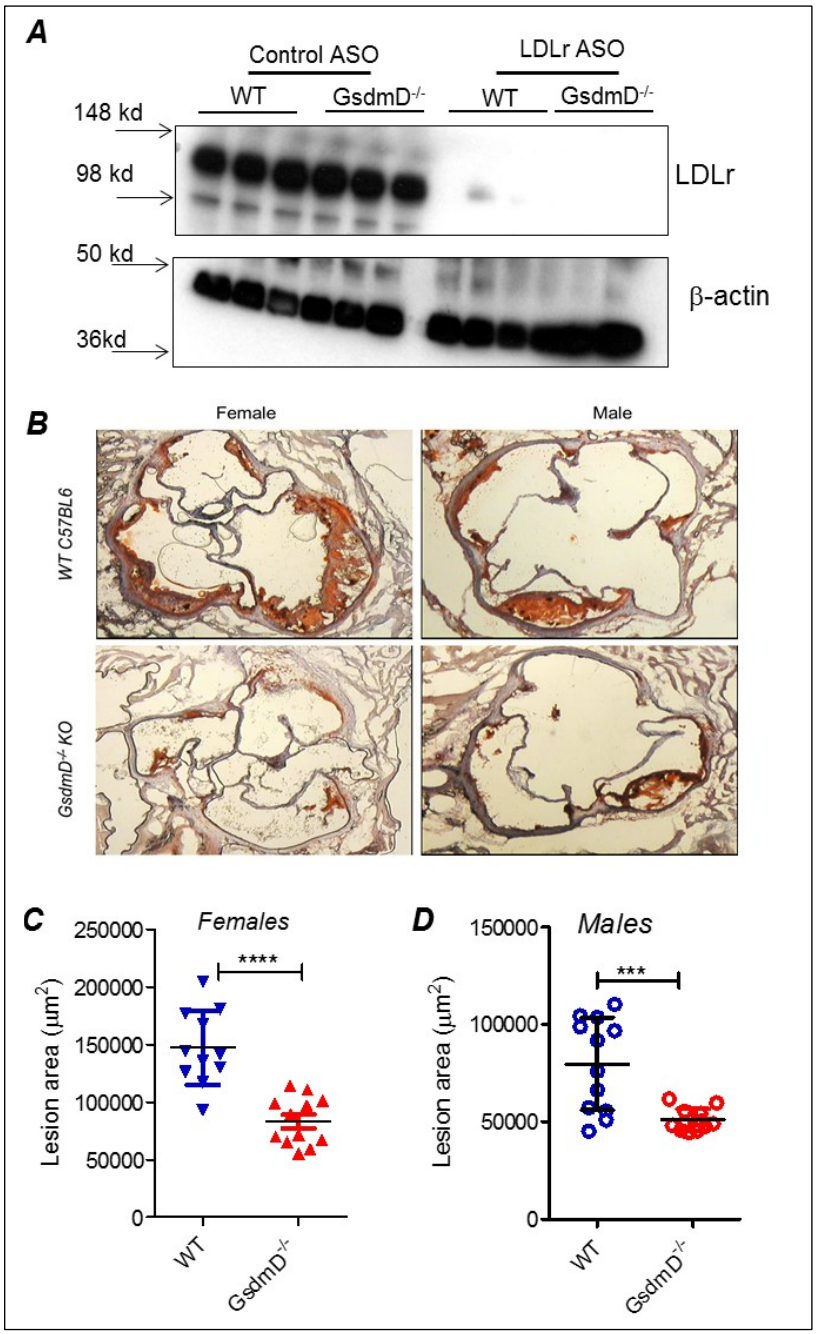

Figure 7